[1]N.Sudarchikova [1]U.Mikolajewicz [1]C.Timmreck [2]D.O'Donnell [3,*]G.Schurgers [4]D.Sein [5]K.Zhang

Modelling of mineral dust for interglacial and glacial climate conditions with focus on Antarctica

Max-Planck-Institute for Meteorology, Hamburg, Germany

Finnish Meteorological Institute, Helsinki, Finland

Department of Physical Geography and Ecosystem Science, Lund University, Sweden

Alfred-Wegener-Institute, Bremerhaven, Germany

Pacific Northwest National Laboratory, Richland, WA

now at: Department of Geosciences and Natural Resource Management, University of Copenhagen, Denmark

Correspondence to: N. Sudarchikova (natalia.sudarchikova@mpimet.mpg.com)

1

Abstract

The mineral dust cycle responds to climate variations and plays an important role in the climate system by affecting the radiative balance of the atmosphere and modifying bio-geochemistry. Polar ice cores provide unique information about deposition of aeolian dust particles transported over long distance. These cores are a paleoclimate proxy archive of climate variability thousands of years ago. The current study is a first attempt to simulate past interglacial dust cycles with a global aerosol-climate model ECHAM5-HAM. The results are used to explain the dust deposition changes in Antarctica in terms of quantitative contribution of different processes, such as emission, atmospheric transport and precipitation, which will help to interpret paleodata from Antarctic ice cores. The investigated periods include four interglacial time-slices: the pre-industrial control (CTRL), mid-Holocene (6000 yr BP), last glacial inception (115 000 yr BP) and Eemian (126 000 yr BP). One glacial time interval, the Last Glacial Maximum (LGM) (21 000 yr BP) was simulated as well to be a reference test for the model. Results suggest an increase of mineral dust deposition globally, and in Antarctica, in the past interglacial periods relative to the pre-industrial CTRL simulation. Approximately two thirds of the increase in the mid-Holocene and Eemian is attributed to enhanced Southern Hemisphere dust emissions. Slightly strengthened transport efficiency causes the remaining one third of the increase in dust deposition. The moderate change of dust deposition in Antarctica in the last glacial inception period is caused by the slightly stronger poleward atmospheric transport efficiency compared to the pre-industrial. Maximum dust deposition in Antarctica was simulated for the glacial period. LGM dust deposition in Antarctica is substantially increased due to 2.6 times higher Southern Hemisphere dust emissions, two times stronger atmospheric transport towards Antarctica, and 30 % weaker precipitation over the Southern Ocean. The model is able to reproduce the order of magnitude of dust deposition globally and in Antarctica for the pre-industrial and LGM climates.

1 Introduction

Desert dust suspended in the atmosphere plays an important role in the climate system. Dust affects climate by changing the radiative balance of the atmosphere through the absorption and scattering of incoming solar and outgoing terrestrial radiation (e.g. Sokolik et al., 2001; Tegen, 2003; Balkanski et al., 2007). Additionally mineral dust may impact climate by modifying cloud properties, acting as cloud condensation nuclei (Twohy et al., 2009; Karydis et al., 2011) or ice nuclei (DeMott, 2003; Liu et al., 2012; Kuebbeler et al., 2014). The atmospheric supply of desert dust is the major source of iron in the open ocean, which is an essential micronutrient for phytoplankton growth and therefore may influence the ocean uptake of atmospheric CO_2 (e.g Martin et al., 1990; Jickells et al., 2005; Wolff et al., 2006; Mahowald et al., 2008). Mineral dust can also act as fertilizer for tropical forests over long time periods (e.g. Okin et al., 2004). In addition, dust can impact atmospheric chemistry via heterogeneous reactions and changes in photolysis rates (e.g. Dentener et al., 1996). Moreover, global aerosol modelling studies suggest that dust is one of the main contributors to the global aerosol burden (Textor et al., 2006).

The main mechanisms controlling dust emissions are vegetation cover, aridity, land surface/soil characteristics, wind speed, precipitation and topographical features. Therefore mineral dust is very sensitive to climate change which has been evidenced by many observational studies (e.g. Kohfeld and Harrison, 2001). Polar ice cores represent unique geological archives of the deposition of aeolian dust particles transported over long distance from desert regions to the polar ice sheets where dust particles are well preserved (Delmonte et al., 2002). Ice core records indicate up to 25 times higher dust deposition rates at high latitudes during glacial periods than in interglacial periods (e.g. Petit et al., 1990, 1999; EPICA Community Members, 2004, 2006). However considering interglacial periods only, some variability of dust also can be noticed (e.g. from the high resolution records in EPICA Community Members, 2006).

For interpretation of paleodust records, a combination of measurements and mod-

elling results can be a fruitful approach. Paleodust records can provide information about the amount, geochemical features and spatial variability of dust in source and deposition regions. The modelling approach is needed for more complete picture involving variations in atmospheric transport of dust and for coverage of places with lack of data.

Simulations of the dust cycle for paleoclimate conditions can give additional insight into past climates, and they also represent a critical test for the models under different climate scenarios, since these simulations can be validated against independent paleo data. One additional aspect is that the simulation of the marine carbon cycle of past time-slices requires adequate dust deposition values as input information for the climate models, which can be derived from model simulations.

Taking into account the impact of different orbital parameters and boundary conditions, four interglacial time-slices, as well as one glacial period, were performed and investigated. The control simulation (CTRL) represents the pre-industrial (interglacial) period. Other interglacial time-slices are the mid-Holocene (6000 yr BP), last glacial inception (115 000 yr BP) and Eemian (126 000 yr BP). The glacial time interval is the Last Glacial Maximum (LGM) (21 000 yr BP). The dust cycle during past interglacial time intervals has not been the subject of many modelling studies (transient EMIC simulation in Bauer and Ganopolski, 2010). Also global dust records covering these periods are rare. For the LGM however, a good precompiled observational based data set on dust deposition is known (DIRTMAP, Kohfeld and Harrison, 2001) and this time-slice has been simulated in several other studies (e.g. Andersen et al., 1998; Werner et al., 2002; Mahowald et al., 1999, 2006; Li et al., 2010; Albani et al., 2012). Thus, in our study we can use results for the LGM simulation as a reference test for the model.

This study is a first attempt to simulate past interglacial dust cycles. The main goals are to analyze the response of the dust cycle to different interglacial and glacial climate conditions and to estimate the quantitative contribution of different processes, such as emission, atmospheric transport and precipitation to dust deposition changes in Antarctica. This is useful for interpretation of the paleo data from Antarctic ice cores.

4

Other important additional aspect of the study is to evaluate the model ability to reproduce the dust cycle under different climate condition by comparing our results with observations and other modelling studies (where available).

In the following sections, we first describe the modelling approach used in the study (Sect. 2). The ability of the model to reproduce the observed dust cycle in pre-industrial period is examined in Sect. 3. Model results and discussion for paleoclimate conditions are the subjects of Sect. 4, in which global and Southern Hemisphere dust emissions are analyzed (Sects. 4.1 and 4.2). Section 4.3 shows the simulated dust deposition with focus on Antarctica for different paleo periods. Comparison of modelled and observed dust deposition fluxes for past interglacial and glacial climate conditions is discussed in Sect. 4.4. The contribution of different processes to dust deposition in Antarctica with emphasis on atmospheric transport efficiency and precipitation is analyzed in Sect. 4.5. Section 5 concludes the main findings of this study.

2   Methods

2.1   Model description

The global aerosol-climate model ECHAM5-HAM (Stier et al., 2005) is used in the current study. The model resolution we use is T31L19, which corresponds to a horizontal resolution of approximately $3.75° \times 3.75°$ and 19 vertical hybrid sigma-pressure levels in the atmosphere (see Table 4 in Roeckner et al. (2006) for details). The aerosol species treated in the model are mineral dust, sulfate, black carbon, organic carbon and sea salt. We focus here on the analysis of the mineral dust cycle. For a detailed description of the model as well as other aerosol species, see Stier et al. (2005). Emitted dust aerosol is represented by two size classes, accumulation and coarse modes with mass-median radii of 0.37 (μm) and 1.75 (μm) and standard deviations of 1.59 and 2.00, respectively. Prognostic variables are aerosol mass and aerosol particle number concentrations for each mode. Emission of mineral dust is calculated online, based

5

on the scheme of Tegen et al. (2002). Dust source regions are arid and semi-arid areas with sparse or no vegetation. The strength of the aeolian emissions depends on surface wind velocity, soil moisture and texture, and snow cover (e.g. Marticorena and Bergametti, 1995; Mahowald et al., 2005). Emissions can take place, when the wind speed reaches a certain threshold friction velocity (Marticorena and Bergametti, 1995). For wind speeds that exceed this threshold, the dust flux is calculated following Tegen et al. (2002). Several soil types (Zobler, 1986) are used in the model. Each soil type is represented by different percentage of soil populations which are characterized by different particle size distribution. Influence of the soil moisture of each soil type on the wind erosion threshold is defined according to Fecan et al. (1999). Aerosol transport is calculated according to Stier et al. (2005).

Sink processes of dust are dry deposition, sedimentation and wet deposition. In this study new changes in wet deposition scheme have been introduced following Verheggen et al. (2007). Scavenging parameter for the mixed and liquid phase clouds parameterization was changed due to a decrease of activated fraction of aerosol particles with increasing cloud ice mass fraction and with decreasing temperature from 0 to $-25\,^{\circ}$C.

2.2 Experimental setup

Vegetation plays an important role in dust modelling because its distribution determines the areas that are potential dust source regions. Present-day and paleoclimatic vegetation conditions were obtained from simulations with the dynamic vegetation model LPJ-GUESS (Smith et al., 2001).

The vegetation model LPJ-GUESS was forced with monthly mean temperature, precipitation and shortwave radiation, obtained from paleoclimate simulations with a coupled climate model (Mikolajewicz et al., 2007), and uses a T31 spatial resolution. The potential dust source regions are defined as regions with annual maximum grass and shrub cover fraction less than or equal to 25 % (modified from Tegen et al., 2002) and shown as light green areas in Fig. 1. The maximum of vegetation cover was used in

6

order to compensate for a slight underestimation of vegetation cover fraction by the LPJ-GUESS model and assuming that even in autumn and winter time, when grass is drying up and leaves are shed, the roots still suppress the emission of soil particles. The basins with pronounced topographic variations are especially favourable for dust mobilization and were taken into account following Ginoux et al. (2001). These areas are called preferential dust source areas and contain large amounts of sediments which are accumulated essentially in the valleys and depressions, and are predominantly silt sized. We applied additional adjustment to the mid-Holocene case due to too high emissions from one particular grid box in South American source and as a consequence overestimated dust deposition in Antarctica. Thus, in order to get reasonable results and better agreement with observations, we suppressed emissions from this grid box and repeated the simulation. Also the vegetation cover in this grid box is almost 25 % which is close to the limit for the definition of potential dust source regions. Hereafter in the text we will refer to this simulation as 6 kyr.

The setup followed the Paleoclimate Modelling Intercomparison Project (PMIP2) protocol (http://pmip2.lsce.ipsl.fr/, Braconnot et al., 2007). For all interglacial time periods current topography and ice sheets were used. For defining the orographic changes in the LGM, the 5 min data set of reconstructed ice sheet topography from PMIP2 (Peltier, 2004), aggregated to a T31 grid was used.

Orbital parameters and greenhouse gas concentrations for the Holocene and LGM simulations were prescribed following the PMIP2 protocol (Table 1). For the time slices 115 kyr and 126 kyr insolation was changed accordingly, greenhouse gas concentrations were kept at pre-industrial level. Monthly mean sea surface temperature (SST), sea ice concentration and surface background albedo for each time-slices were obtained from the long-term simulation with the coupled atmosphere ocean dynamical vegetation model ECHAM5/MPIOM/LPJ (Mikolajewicz et al., 2007). Sea surface temperatures were corrected for the systematic error of the coupled run by adding the SST differences between observed and simulated SSTs for the pre-industrial period (similar to Arpe et al., 2011). SST's thus prescribed for the paleo time-slice simulations are,

7

on a global average, lower by $-0.07\,°C$ in $6\,kyr$, by $-0.08\,°C$ in $115\,kyr$, by $-0.13\,°C$ in $126\,kyr$ and by $-2.7\,°C$ in the LGM compared to the pre-industrial SST. In this study the results from $20\,yr$ time-slice simulations after $5\,yr$ of spin up have been analyzed.

3   Model results for the pre-industrial climate conditions

First of all we estimated the ability of the model, using a prescribed pre-industrial modelled vegetation map, to reproduce modern dust deposition flux (Fig. 2). Dust deposition records include ice core measurements, expressed as deposition fluxes and marine sediment core records and represent averages for the Holocene period or shorter periods within that interval. The data are derived from "Dust Indicators and Records of Terrestrial and Marine Palaeoenvironments" data base (DIRTMAP, Kohfeld and Harrison, 2001).

The model is able to reproduce the general patterns and capture the large range of five orders of magnitude of the observed dust deposition flux within an order of magnitude (Fig. 2). The correlation coefficient of the natural logarithm of the observed and modelled values is 0.78. In the polar regions a discrepancy between the simulated and available observed dust deposition occurs in the northern high-latitudes in Greenland, where the model overestimates the observed values by a factor of about 3–10. A similar bias is also reported in the modelling study by Mahowald et al. (1999). Some difficulties arise in validating the model for the Southern Hemisphere due to lack of datasets in these latitudes. In Antarctica the model overestimates observed values by a factor of about 2–3 due to the overestimation of the Australian dust source, as well as due to too high wet deposition in the Antarctica interior. At the same time, the model underestimates the dust deposition in the Weddell Sea close to Antarctica, which was also reported in other global modelling studies (e.g. Huneeus et al., 2011).

The simulated seasonal cycle of dust deposition in different sites in Antarctica shows general agreement with the observations. Observations at James Ross Island station show a maximum dust deposition in late austral winter (Mcconnell et al., 2007), which

is close to the simulated spring maximum at that site. Similarly, the simulated maximum dust deposition at the Berkner Island site is in spring, while observations show a spring/summer maximum (Bory et al., 2010). The recorded annual cycle of dust deposition at Law Dome shows spring and autumn maximum (Burn-Nunes et al., 2011). In our simulation dust deposition at Law Dome shows a maximum during spring and summer seasons.

The global mean dust emission for the pre-industrial control simulation is $1540\,\mathrm{Tg\,yr^{-1}}$. This value is in fairly good agreement with the total dust emissions generated by the pre-industrial model runs within the aerosol model intercomparison project (AeroCom), which lie between 1570 and $1700\,\mathrm{Tg\,yr^{-1}}$ (http://aerocom.met.no). Dust emissions from the Southern Hemisphere contribute less than 10 % to the global emissions, but are the main sources of dust deposited in Antarctica. Simulated dust emissions from Australia amount to $60\,\mathrm{Tg\,yr^{-1}}$, which is in the range of 15 different models with modern climate conditions within the AeroCom project (Huneeus et al., 2011). Dust mobilization from South America is rather small and lies close to the low end of the AeroCom model simulations. The South African source is also weak and underestimated compared to other models.

Simulated dust emissions from Australia start to increase in October and reach their maximum in November–December, showing equally high emissions in SON and DJF (not shown). This is in general agreement with satellite observations, suggesting the start of Australian dust mobilization is in September–October and its maximum is in December–February (Prospero, 2002). Observations over southern Africa show maximum emissions in August–October, while the modelled maximum emissions are shifted to November–January. The modelled seasonal cycle of South American dust emissions is in general agreement with observations and shows maximum activity in October–November.

In the model simulation wet deposition is the dominant sink process of dust over Antarctica, which is similar to the modelling study of Albani et al. (2012). However, observations in high-latitude polar regions at inland sites suggest dry deposition as

9

the dominant sink process (e.g. Legrand and Mayewski, 1997; De Angelis et al., 1997) and wet deposition can be a major sink process for the coastal Antarctic sites (e.g. Wolff et al., 1998). Modelled snow accumulation in Antarctic sites, and thus processes responsible for wet deposition, are overestimated by a factor of about 1.5–2.5.

In the next section we will discuss paleo time-slice simulations relative to pre-industrial results.

4   Model results and discussion for paleoclimate conditions

4.1   Global dust emissions

Global dust emissions are higher by 27 %, 23 % and 55 % for 6 kyr, 115 kyr and 126 kyr respectively and by a factor of 2 for the LGM compared to the CTRL simulation (Table 2). The changes are mainly due to strengthening of the Northern Hemisphere dust sources. In 126 kyr (less pronounced in 6 kyr) the increase of total emissions is mainly attributed to the Ustyurt Plateau source (Central Asia). In 115 kyr the increase of emissions is largest in Sahara due to the weakening of African summer monsoons and as a consequence an extension of the Saharan dust source (Fig. 1). The simulated enlargement of emissions in the glacial period is consistent with other modelling studies (e.g. Werner et al., 2002). Mahowald et al. (2006) reported an increase in LGM dust emissions from 2.2 times current climate to 3.3 after including the glaciogenic dust sources (generated by continental ice sheets) in the LGM simulation.

4.2   Southern Hemisphere dust emissions

Southern Hemisphere dust emissions are dominated by the Australian dust source in all interglacial simulations (Fig. 3). In the LGM, the southern South American dust source is of equal importance to the Australian one. Note that we did not include glaciogenic dust sources in the LGM simulation, one of which is located in South America, Pampas region (Mahowald et al., 2006).

10

Australian emissions in 6 kyr and 126 kyr are higher compared to the CTRL simulation by a factor of 1.9 and 1.8 respectively. Most of the increase in 126 kyr is caused by an enlarged source area extent (by about factor of 1.8) as a consequence of dry austral summers. In 6 kyr and 115 kyr the Australian dust source area extent is reduced by almost one half of the source area in CTRL. The increase of Australian emissions in 6 kyr is related to more frequent high wind speed and low soil wetness in the western part of Australia. In 115 kyr, drier soil combined with an almost unchanged wind speed distribution effectively cancels out the effect of the reduced source area previously noted, resulting in an emission flux similar to that in CTRL. According to the simulations, the dust source areas and emissions in South America are quite persistent through all interglacial time-slices. The dust emissions from the south African source are stable in considered time-slice simulations, consistent with the frequency of high wind speed.

The main increase in Southern Hemisphere emissions is found in the LGM due to the significantly strengthened South American dust source. This is caused by both an extended dust source area and a much higher probability of high wind speed over the additional source area, which is formed in the LGM. Furthermore increased emissions are also related to regionally reduced soil wetness and particularly dry soil in the "new" source areas in the south of Patagonia region. Emissions from the Australian dust source are slightly increased in the LGM with respect to the pre-industrial time-slice. This results from an enlarged dust source area extent and regionally lower soil wetness, while the probability of high wind speed over Australian sources is similar to that in the CTRL run.

4.3 Dust deposition with focus on Antarctica

The increase of global dust mobilization in paleoclimate conditions, which was discussed previously, is reflected in enhanced dust deposition compared to the pre-industrial period (Fig. 4). In all time-slice simulations, sedimentation and wet deposition are the main global loss processes of mineral dust accounting each for more than 40 % of the total dust removal, except for 126 kyr. In 126 kyr the relative contribution of sedi-

mentation to the total sink is weaker, due to increased tropical monsoonal activity and consequently wet deposition close to the main dust source regions in Asia and the Sahara. Wet deposition is slightly reduced in relative strength in the LGM compared to CTRL due to the drier climate conditions. Dry deposition is also a significant sink process, accounting for $14 \pm 1\,\%$ of dust removal.

Simulated dust deposition over Antarctica is higher by a factor of 2.8 and 2.7 in 6 kyr and 126 kyr respectively, and slightly larger in 115 kyr with respect to CTRL. The maximum dust deposition is found in the LGM showing a 10-fold increase which is similar to the other modelling study (Albani et al., 2012). The relative contribution of dry deposition in Antarctica at LGM is increased, but the model still overestimates wet deposition in that region. Modelled glacial snow accumulation in Antarctic sites is higher compared to observations by a factor of about 1.2–2, which is similar to the overestimation of precipitation in the pre-industrial period.

Regarding the seasonality of dust concentration in Antarctic ice, the model results suggest the maximum in austral spring (SON) for all interglacial time-slices. However, for the LGM the geographical patterns of seasonal maximum dust concentration in ice are more complicated and depend on the region (not shown).

In the next section the modelled dust deposition in the LGM and past interglacial time-slices are compared with observations.

4.4   Model results versus observations: dust deposition in paleoclimate conditions

4.4.1   Last Glacial Maximum

To compare model results with observations the DIRTMAP database (Kohfeld and Harrison, 2001) was used. The absolute magnitude of the observed (circles) and modelled LGM dust deposition rates are shown in Fig. 5 (top). Both dust deposition records and modelled data at the LGM show deposition fluxes that are generally higher than in the current climate. A scatter plot of the observed versus modelled dust fluxes (Fig. 5, bot-

12

tom) for the LGM shows that the model is able to capture the high- and low-deposition regions. The correlation coefficient of the natural logarithm of the observed and modelled values for the LGM is 0.81. The model overestimates observed deposition flux on the coasts of Greenland and slightly underestimates it at an inland site. The model is in good agreement with observations from Byrd station (western Antarctica). On the East Antarctic Plateau the model underestimates LGM dust deposition by a factor of about 4–5.

4.4.2 Interglacial time periods

There are not many data sets of dust records existing which cover the considered time periods. Moreover comparison of the model results against observations for 6 kyr period is a nontrivial task because many of the available records represent the average for the Holocene (0–10 kyr) and assume that these data represent the current climate. However some continuous measurements from ice cores and marine cores can be found in the literature. To compare modelled results with observations for the past interglacial periods the ice core records in Antarctica were used. These are Vostok (78°28′ S, 106°50′ E) (Petit et al., 1999), EPICA Dome C (EDC, 75°06′ S, 123°21′ E) (Lambert et al., 2012), EPICA Dronning Maud Land (EDML, 75°00′ S, 00°04′ E) (A. Wegner, personal communication, 2010) and Talos Dome ice core (TALDICE, 72°70′ S, 159°11′ E) (Schupbach et al., 2013). The sites locations are shown in Fig. 6.

The records of dust deposition flux, as mean values for the intervals $6 \pm 1\,\mathrm{kyr}$, $115 \pm 1\,\mathrm{kyr}$ and $126 \pm 1\,\mathrm{kyr}$ relative to the values averaged for the period 0–4.5 kyr (or shorter period within this interval) from corresponding ice cores, are shown in Fig. 7. The observations show a general increase of dust deposition for the past interglacial intervals compared to pre-industrial values, with maximal increase in 126 kyr. The model results are close to the observed values in some cases, but can differ by a factor of up to 3 in others. Overestimated 6 kyr to pre-industrial ratios are likely due to too high emissions from Australian source in 6 kyr. The underestimation in Vostok in 115 kyr and 126 kyr could be a consequence of the underestimated South American dust source. Very

13

strong emissions from the Australian source in 6 kyr and 126 kyr causes an overestimation of the dust deposition at EDC site in these time slices.

4.5 Contribution of different processes to dust deposition in Antarctica

As mentioned before, dust deposition in Antarctica is nonlinearly related to a number of factors such as Southern Hemisphere dust emissions, atmospheric transport and the hydrological cycle. Figure 8a demonstrates that simulated Southern Hemisphere dust emissions with a seasonal maximum in austral summer (DJF) and spring (SON) under interglacial and glacial climate conditions can only partly explain the relative amount and seasonality of dust deposition in Antarctica (Fig. 8b). The main focus of this section is to analyze the contribution of the aforementioned processes to dust deposition in Antarctica in different climate conditions by using a modelling approach. With this goal, an analysis method has been developed that describes emission of dust in the Southern Hemisphere, its poleward transport, loss due to precipitation over the ocean south of $40°$ S and final deposition in Antarctica (Fig. 8). Using this method we made an attempt to qualitatively explain seasonal variations of dust deposition between time-slices as well as differences between time-slices.

4.5.1 Atmospheric transport efficiency

One of the possibilities to describe atmospheric transport is by means of air mass trajectories. Air mass trajectories from the Southern Hemisphere dust sources to Antarctica were calculated. To calculate trajectories, 6 hourly data of the meridional, zonal and vertical components of wind from 20 years of simulation were used. Trajectories were calculated once per day. We considered trajectories that originated over the Southern Hemisphere dust sources at the pressure levels of 800 hPa and 500 hPa and reached Antarctica within 10 days. The three-dimensional passive tracer trajectories were calculated based on bilinearly interpolated velocities. According to Krinner et al. (2010), there are two types of tropospheric tracer transport towards the interior of

14

the Antarctic continent: fast, low-level advection enhanced by cyclonic systems off the Antarctic coast and advection via mass convergence in the middle troposphere above Antarctica. The 500 hPa and 800 hPa pressure levels have therefore been chosen in order to analyze the atmospheric dust transport in the low and middle troposphere. In order to examine atmospheric transport alone, without the influence of the dust source extent which is different in all the simulations, the number of trajectories for each time-slice was normalized with respect to the dust source area extent. An example of trajectories for austral spring originating over the South American, Australian and South African dust sources at 500 hPa and 800 hPa and reaching Antarctica within 10 days for the CTRL simulation is shown in Fig. 9.

Based on the number of trajectories that reach Antarctica, we derived transport efficiency. Our simulations show that low level transport from Australia is more efficient than from South America. In 500 hPa, the picture is opposite, trajectories that originate over South America are more frequent than those originating over Australia. This is similar for all considered interglacial time slices. Delmonte et al. (2007) suggested a mixture of Australian and South American dust as the most probable sources for dust deposition in Antarctica in the Holocene and Eemian. However they note that this hypothesis needs further investigation. At the LGM, both, low- and middle atmosphere transport from South America is more efficient than from Australia.

In general, for the interglacial time-slice simulations, the number of trajectories originating over the Southern Hemisphere dust sources at 800 hPa and reaching Antarctica is about 10 % of the total number of trajectories originating over the Southern Hemisphere dust sources; and the number of trajectories originating at 500 hPa and reaching Antarctica is about 3.5–5 %. The increased meridional temperature gradient at the LGM leads to more efficient poleward transport (Petit et al., 1999) and the number of trajectories reaching Antarctica is higher (13 % for 800 hPa and 7.3 % for 500 hPa) compared to the interglacial time-slices. Another feature of the glacial period is a weaker seasonality of poleward transport compared to the interglacial time-slices (Fig. 8c). The poleward atmospheric transport for all considered time-slices is more active in austral

15

winter (JJA) and minimal in summer (DJF) (Fig. 8c), similar to the results from Krinner et al. (2010), who compared model results for LGM and present day. This implies that seasonality of Southern Hemisphere dust mobilization and atmospheric transport towards Antarctica are out of phase.

Regarding dust deposition in Antarctica, the transport strength is most important for the seasons with largest Southern Hemisphere dust emissions (SON and DJF). Analysis shows a slight increase of poleward transport in the corresponding seasons in 6 kyr and 126 kyr. The increase is attributed to the southward deflection of the transport pathway over the Weddell Sea in 6 kyr and over the Ross Sea region in 126 kyr (Fig. 10). Our results suggest slightly more active atmospheric transport in 115 kyr compared to other interglacial time-slices which is in agreement with the modelling study by Krinner and Genthon (2003) for present and 115 kyr. According to our model results this can be explained by somewhat enhanced cyclonic activity in most of the seasons (not shown). This seems to be consistent with the ice core data (Petit et al., 1999; Wolff et al., 2006) which show an increase of sea salt concentration at 115 kyr, as an indicator of greater cyclonic activity over the open ocean (Petit and Delmonte, 2009). The slight strengthening of the atmospheric transport in 115 kyr results only in a moderate increase of dust concentration in Antarctica compared to pre-industrial according to the model.

The poleward transport for both, the low- and middle atmosphere is found to be more efficient at the LGM (by about factor of 2 compared to pre-industrial), in particular in austral summer. The strengthened low-level transport is consistent with findings from Krinner and Genthon (2003) who indicated a more frequent fast low-level tracer advection towards Antarctica as a consequence of the more vigorous meridional eddy transport and of the increased vertical atmospheric stability during the LGM. However, contrary to our study, they suggested a lower fraction of tracers advected via the upper-level pathways in the LGM than in present. A possible reason for this disagreement could be related to different trajectory analysis. Krinner and Genthon (2003) considered the tracers originating above 400 hPa over the Southern Ocean between 50 and

70° S in contrast with our trajectories that originate above the Southern Hemisphere dust sources (~ 20–$50°$ S) at 500 hPa.

In order to understand which mechanism is responsible for the poleward transport change, dust flux for different climate conditions at 500 hPa was calculated by using monthly mean (not shown) and 6 hourly data (Fig. 10). Dust flux calculated with monthly mean data shows that the mean transport at high southern latitudes is dominated by zonal circulation and very similar for all time-slices. However, dust flux calculated by using 6 hourly data shows an increase of meridional contribution and significant changes in the dust transport patterns towards Antarctica between different time-slices due to synoptic variability. Thus, the transport pathway change in different time-slices is due to synoptic variability. The relative contribution of dust transport at 40–70° N due to synoptic variability to the mean (total) meridional transport is about 70–90 % in interglacial time-slices and nearly 100 % in the LGM.

Multiplying the Southern Hemisphere dust emissions with the number of trajectories leading to Antarctica defines a quantity, which we call potential dust transport (in arbitrary units) (Fig. 8d). This gives some idea about both, how much dust is emitted and how often dust is transported to Antarctica. However these factors alone cannot explain the modelled dust deposition changes (Fig. 8b).

4.5.2 Precipitation

Precipitation is an important process as it is one of the removal mechanisms for atmospheric particles on the transportation pathway. Interglacial time-slices show just a moderate change in precipitation over the ocean south of 40° S, while LGM precipitation is about 30 % weaker compared to the pre-industrial time-slice (Figs. 11 and 8e). This favours the increase of dust deposition in Antarctica in glacial periods. Moreover, LGM precipitation over Antarctica is approximately half the pre-industrial precipitation, which alone leads to about doubling of the dust concentration in ice (not shown).

The seasonal influence of precipitation can be seen in MAM (Fig. 8e). Relatively strong dust transport efficiency is affected by seasonal maximum precipitation (over

17

the ocean south of 40° S), which results in seasonal minimum deposition in Antarctica (Fig. 8b). This is valid for all interglacial time-slices. In the LGM, the seasonality of dust deposition over Antarctica in MAM and JJA is affected by precipitation in a different way. This probably results from an increased fraction of snowfall, compared to rain in the LGM over the Southern Ocean, and different scavenging efficiency coefficients for snow and liquid in the model. According to Stier et al. (2005), liquid precipitation removes aerosol more efficiently than snow.

5 Summary and conclusions

This study presents the first attempt to simulate past interglacial dust cycles with a global aerosol-climate model. The work aims to investigate the variations of dust deposition in Antarctica in terms of quantitative contribution of different processes, such as dust emission, atmospheric transport and precipitation in order to help interpret paleo records of dust from Antarctic ice cores. The four interglacial time periods analyzed include the pre-industrial control (CTRL), mid-Holocene (6000 yr BP), last glacial inception (115 000 yr BP) and Eemian (126 000 yr BP) simulations. One glacial time interval, which is Last Glacial Maximum (LGM) (21 000 yr BP), was simulated as well, as a reference test for the model.

The model is able to capture the large range of five orders of magnitude of the observed dust deposition flux within an order of magnitude for pre-industrial and LGM climate conditions. Underestimation of glacial values in Eastern Antarctica can most likely be attributed to the comparable weak source in southern South America. Including glaciogenic dust sources in the Pampas region (Mahowald et al., 2006) would enhance the South American dust source and could improve the agreement with observations. The increase of spatial model resolution could be important for a better representation of the southern South American dust source as well. Records from Antarctic ice cores for interglacial time periods indicate slightly higher dust deposition flux compared to pre-industrial values. The model results are close to the observed

18

values in some cases, but can differ by a factor of up to 3 in others. The model is very sensitive to vegetation cover and thus it is the main source of uncertainties in our study.

Our results suggest the increase of dust deposition in Antarctica for all considered time-slices relative to the pre-industrial period. In the mid-Holocene and Eemian dust deposition is increased by a factor of 2.8 and 2.7 respectively. Approximately two thirds of the increase in both periods is attributed to enhanced Southern Hemisphere dust emissions. Slightly strengthened transport efficiency due to southward deflection of the transport pathway causes the remaining one third of the increase in dust deposition. Compared to pre-industrial conditions, more intensive poleward transport at 115 kyr together with almost similar Southern Hemisphere emissions results in only slightly enhanced dust deposition in Antarctica. The highest dust deposition in Antarctica is simulated for the LGM, showing a 10.2-fold increase compared to CTRL. This results from a combination of 2.6 times higher Southern Hemisphere dust emissions, two times stronger transport and 30 % weaker precipitation over the Southern Ocean. Our finding supports suggestion of other studies (e.g., Krinner et al., 2010; Krinner and Genthon, 2003) towards more intensive atmospheric poleward transport during glacial period.

Similar to Krinner et al. (2010) who analyzed model results for LGM and present day, our results show that poleward atmospheric transport is more vigorous in JJA and MAM DJF for all simulated time periods. This implies that seasonality of atmospheric transport towards Antarctica and Southern Hemisphere dust emissions (with a peak in SON and DJF) are in general out of phase.

References

Albani, S., Mahowald, N. M., Delmonte, B., Maggi, V., and Winckler, G.: Comparing modelled and observed changes in mineral dust transport and deposition to Antarctica between the Last Glacial Maximum and current climates, Clim. Dynam., 38, 1731–1755, 2012.

Andersen, K. K., Armengaud, A., and Genthon, C.: Atmospheric dust under glacial and interglacial conditions, Geophys. Res. Lett., 25, 2281–2284, 1998.

Arpe, K., Leroy, S. A. G., and Mikolajewicz, U.: A comparison of climate simulations for the last glacial maximum with three different versions of the ECHAM model and implications for summer-green tree refugia, Clim. Past, 7, 91–114, 10.5194/cp-7-91-2011, 2011.

Balkanski, Y., Schulz, M., Claquin, T., and Guibert, S.: Reevaluation of Mineral aerosol radiative forcings suggests a better agreement with satellite and AERONET data, 7, 81–95, 2007.

Basile, I., Grousset, F. E., Revel, M., Robert, J., Biscaye, P. E., and Barkov, N. I.: Patagonian origin of glacial dust deposited in East Antarctica (Vostok and Dome C) during glacial stages 2, 4 and 6, 146, 573–589, 1997.

Bauer, E. and Ganopolski, A.: Aeolian dust modelling over the past four glacial cycles with CLIMBER-2, Global Planet. Change, 74, 49–60, 10.1016/j.gloplacha.2010.07.009, 2010.

Bory, A., Wolff, E., Mulvaney, R., Jagoutz, E., Wegner, A., Ruth, U., and Elderfield, H.: Multiple sources supply eolian mineral dust to the Atlantic sector of coastal Antarctica: evidence from recent snow layers at the top of Berkner Island ice sheet, Earth Planet. Sc. Lett., 291, 138–148, 10.1016/j.epsl.2010.01.006, 2010.

Braconnot, P., Otto-Bliesner, B., Harrison, S., Joussaume, S., Peterchmitt, J.-Y., Abe-Ouchi, A., Crucifix, M., Driesschaert, E., Fichefet, Th., Hewitt, C. D., Kageyama, M., Kitoh, A., Laîné, A., Loutre, M.-F., Marti, O., Merkel, U., Ramstein, G., Valdes, P., Weber, S. L., Yu, Y., and Zhao, Y.: Results of PMIP2 coupled simulations of the Mid-Holocene and Last Glacial Maximum – Part 1: experiments and large-scale features, Clim. Past, 3, 261–277, 10.5194/cp-3-261-2007, 2007.

Burn-Nunes, L. J., Vallelonga, P., Loss, R. D., Burton, G. R., Moy, A., Curran, M., Hong, S., Smith, A. M., Edwards, R., Morgan, V. I., and Rosman, K. J.: Seasonal variability in the input of lead, barium and indium to Law Dome, Antarctica, Geochim. Cosmochim. Ac., 75, 1–20, 10.1016/j.gca.2010.09.037, 2011.

De Angelis, M., Steffensen, J. P., Legrand, M., Clausen, H., and Hammer, C.: Primary aerosol (sea salt and soil dust) deposited in Greenland ice during the last climatic cycle: comparison

with east Antarctic records, J. Geophys. Res., 102, 26681, 10.1029/97JC01298, 1997.

Delmonte, B., Petit, J., and Maggi, V.: Glacial to Holocene implications of the new 27000-year dust record from the EPICA Dome C (East Antarctica) ice core, Clim. Dynam., 18, 647–660, 10.1007/s00382-001-0193-9, 2002.

Delmonte, B., Petit, J., Basile-Doelsch, I., Jagoutz, E., and Maggi, V.: Late quaternary interglacials in East Antarctica from ice-core dust records, in: The Climate of Past Interglacials, Developments in Quaternary Science, Vol. 7, 54–73, 2007.

Delmonte, B., Andersson, P., Schöberg, H., Hansson, M., Petit, J., Delmas, R., Gaiero, D., Maggi, V., and Frezzotti, M.: Geographic provenance of aeolian dust in East Antarctica during Pleistocene glaciations: preliminary results from Talos Dome and comparison with East Antarctic and new Andean ice core data, Quaternary Sci. Rev., 29, 256–264, 10.1016/j.quascirev.2009.05.010, 2010a.

Delmonte, B., Baroni, C., Andersson, P. S., Schoberg, H., Hansson, M., Aciego, S., Petit, J.-R., Albani, S., Mazzola, C., Maggi, V., and Frezzotti, M.: Aeolian dust in the Talos Dome ice core (East Antarctica, Pacific/Ross Sea sector): Victoria Land versus remote sources over the last two climate cycles, J. Quaternary Sci., 25, 1327–1337, 10.1002/jqs.1418, 2010b.

DeMott, P. J.: African dust aerosols as atmospheric ice nuclei, Geophys. Res. Lett., 30, 1732, 10.1029/2003GL017410, 2003.

Dentener, F. J., Carmichael, G. R., Zhang, Y., Lelieveld, J., and Crutzen, P. J.: Role of mineral aerosol as a reactive surface in the global troposphere, J. Geophys, Res., 101, 22869–22889, 1996.

EPICA Community Members: Eight glacial cycles from an Antarctic ice core, Nature, 429, 623–628, 10.1038/nature02599, 2004.

EPICA Community Members: One-to-one coupling of glacial climate variability in Greenland and Antarctica, Nature, 444, 195–198, 10.1038/nature05301, 2006.

Fécan, F., Marticorena, B., and Bergametti, G.: Parametrization of the increase of the aeolian erosion threshold wind friction velocity due to soil moisture for arid and semi-arid areas, Ann. Geophys., 17, 149–157, 10.1007/s00585-999-0149-7, 1999.

Ginoux, P., Chin, M., Tegen, I., Prospero, J. M., Holben, B., and Dubovik, O.: Sources and distributions of dust aerosols simulated with the GOCART model, J. Geophys. Res., 106, 20255–20273, 2001.

Grousset, F. E., Biscaye, P. E., Revel, M., Petit, J.-R., Pye, K., Joussaume, S., and Jouzel, J.: Antarctic (Dome C) ice-core dust at 18 k.y. B. P.: Isotopic constraints on origins, Earth Planet.

Sc. Lett., 111, 175–182, 10.1016/0012-821X(92)90177-W, 1992.

Huneeus, N., Schulz, M., Balkanski, Y., Griesfeller, J., Prospero, J., Kinne, S., Bauer, S., Boucher, O., Chin, M., Dentener, F., Diehl, T., Easter, R., Fillmore, D., Ghan, S., Ginoux, P., Grini, A., Horowitz, L., Koch, D., Krol, M. C., Landing, W., Liu, X., Mahowald, N., Miller, R., Morcrette, J.-J., Myhre, G., Penner, J., Perlwitz, J., Stier, P., Takemura, T., and Zender, C. S.: Global dust model intercomparison in AeroCom phase I, Atmos. Chem. Phys., 11, 7781–7816, 10.5194/acp-11-7781-2011, 2011.

Jickells, T. D., An, Z. S., Andersen, K. K., Baker, A. R., Bergametti, G., Brooks, N., Cao, J. J., Boyd, P. W., Duce, R. A., Hunter, K. A., Kawahata, H., Kubilay, N., LaRoche, J., Liss, P. S., Mahowald, N., Prospero, J. M., Ridgwell, A. J., Tegen, I., and Torres, R.: Global iron connections between desert dust, ocean biogeochemistry, and climate, Science, 308, 67–71, 10.1126/science.1105959, 2005.

Karydis, V. A., Kumar, P., Barahona, D., Sokolik, I. N., and Nenes, A.: On the effect of dust particles on global cloud condensation nuclei and cloud droplet number, J. Geophys. Res., 116, D23204, 10.1029/2011JD016283, 2011.

Kohfeld, K. E. and Harrison, S. P.: DIRTMAP: the geological record of dust, Earth-Sci. Rev., 54, 81–114, 10.1016/S0012-8252(01)00042-3, 2001.

Krinner, G. and Genthon, C.: Tropospheric transport of continental tracers towards Antarctica under varying climatic conditions, Tellus B, 55, 54–70, 10.1034/j.1600-0889.2003.00004.x, 2003.

Krinner, G., Petit, J.-R., and Delmonte, B.: Altitude of atmospheric tracer transport towards Antarctica inpresent and glacial climate, Quaternary Sci. Rev., 29, 274–284, 10.1016/j.quascirev.2009.06.020, 2010.

Kuebbeler, M., Lohmann, U., Hendricks, J., and Kärcher, B.: Dust ice nuclei effects on cirrus clouds, Atmos. Chem. Phys., 14, 3027–3046, 10.5194/acp-14-3027-2014, 2014.

Lambert, F., Delmonte, B., Petit, J. R., Bigler, M., Kaufmann, P. R., Hutterli, M. A., Stocker, T. F., Ruth, U., Steffensen, J. P., and Maggi, V.: Dust-climate couplings over the past 800,000 years from the EPICA Dome C ice core, Nature, 452, 616–9, 10.1038/nature06763, 2008.

Lambert, F., Bigler, M., Steffensen, J. P., Hutterli, M. A., and Fischer, H.: Centennial mineral dust variability in high-resolution ice core data from Dome C, Antarctica, Clim. Past, 8, 609–623, 10.5194/cp-8-609-2012, 2012.

Legrand, M. and Mayewski, P.: Glaciochemistry of polar ice cores: a review, Rev. Geophys., 35, 219–243, 1997.

22

Li, F., Ramaswamy, V., Ginoux, P., Broccoli, A. J., Delworth, T., and Zeng, F.: Toward understanding the dust deposition in Antarctica during the Last Glacial Maximum: sensitivity studies on plausible causes, J. Geophys. Res., 115, D24120, 10.1029/2010JD014791, 2010.

Liu, X., Shi, X., Zhang, K., Jensen, E. J., Gettelman, A., Barahona, D., Nenes, A., and Lawson, P.: Sensitivity studies of dust ice nuclei effect on cirrus clouds with the Community Atmosphere Model CAM5, Atmos. Chem. Phys., 12, 12061–12079, 10.5194/acp-12-12061-2012, 2012.

Mahowald, N., Kohfeld, K., Hansson, M., Balkanski, Y., Harrison, S. P., Prentice, I. C., Schulz, M., and Rodhe, H.: Dust sources and deposition during the last glacial maximum and current climate: a comparison of model results with paleodata from ice cores and marine sediments, J. Geophys. Res., 104, 15895–15916, 10.1029/1999JD900084, 1999.

Mahowald, N., Jickells, T. D., Baker, A. R., Artaxo, P., Benitez-Nelson, C. R., Bergametti, G., Bond, T. C., Chen, Y., Cohen, D. D., Herut, B., Kubilay, N., Losno, R., Luo, C., Maenhaut, W., McGee, K. A., Okin, G. S., Siefert, R. L., and Tsukuda, S.: Global distribution of atmospheric phosphorus sources, concentrations and deposition rates, and anthropogenic impacts, Global Biogeochem. Cy., 22, GB4026, 10.1029/2008GB003240, 2008.

Mahowald, N. M., Baker, A. R., Bergametti, G., Brooks, N., Duce, R. A., Jickells, T. D., Kubilay, N., Prospero, J. M., and Tegen, I.: Atmospheric global dust cycle and iron inputs to the ocean, Global Biogeochem. Cy., 19, 10.1029/2004GB002402, 2005.

Mahowald, N. M., Muhs, D. R., Levis, S., Rasch, P. J., Yoshioka, M., Zender, C. S., and Luo, C.: Change in atmospheric mineral aerosols in response to climate: Last glacial period, preindustrial, modern, and doubled carbon dioxide climates, J. Geophys. Res., 111, D10202, 10.1029/2005JD006653, 2006.

Marticorena, B. and Bergametti, G.: modelling the atmospheric dust cycle: 1. Design of a soil-derived dust emission scheme, J. Geophys. Res., 100, 16415–16430, 10.1029/95JD00690, 1995.

Martin, J. H., Gordon, R. M., and Fitzwater, S. E.: Iron in Antarctic waters, Nature, 345, 156–158, 1990.

Mcconnell, J. R., Aristarain, A. J., Banta, J. R., Edwards, P. R., and Simes, J. C.: 20th-Century doubling in dust archived in an Antarctic Peninsula ice core parallels climate change and desertification in South America, P. Natl. Acad. Sci. USA, 104, 5743–5748, 2007.

Mikolajewicz, U., Vizcaíno, M., Jungclaus, J., and Schurgers, G.: Effect of ice sheet interactions in anthropogenic climate change simulations, Geophys. Res. Lett., 34, L18706,

10.1029/2007GL031173, 2007.

Okin, G. S., Mahowald, N., Chadwick, O. A., and Artaxo, P.: Impact of desert dust on the biogeochemistry of phosphorus in terrestrial ecosystems, Global Biogeochem. Cy., 18, 10.1029/2003GB002145, 2004.

Peltier, W.: Global glacial isostasy and the surface of the ice-age-Earth: the ICE-5G (VM2) model and GRACE, Annu. Rev. Earth Pl. Sc., 32, 111–149, 10.1146/annurev.earth.32.082503.144359, 2004.

Petit, J. R. and Delmonte, B.: A model for large glacial-interglacial climate-induced changes in dust and sea salt concentrations in deep ice cores (central Antarctica): palaeoclimatic implications and prospects for refining ice core chronologies, Tellus B, 61, 768–790, 10.1111/j.1600-0889.2009.00437.x, 2009.

Petit, J. R., Mounier, L., Jouzel, J., Korotkevich, Y. S., Kotlyakov, V. I., and Lorius, C.: Palaeo-climatological and chronological imolications of the Vostok core dust record, Nature, 343, 56–58, 1990.

Petit, J. R., Jouyel, J., Raynaud, D., Barkov, N. I., Barnova, J.-M., Basile, I., Bender, M., Chappellaz, J., Davis, M., Delaygue, G., Delmotte, M., Kotlyakov, V. M., Legrand, M., Lipenkov, V. Y., Lorius, C., Pepin, L., Ritz, C., Saltzman, E., and Stievenard, M.: Climate and atmospheric history of the past 420,000 years from the Vostok ice core, Antarctica, Nature, 399, 429–436, 1999.

Prospero, J. M.: Environmental characterization of global sources of atmospheric soil dust identified with the NIMBUS 7 Total Ozone Mapping Spectrometer (TOMS) absorbing aerosol product, Rev. Geophys., 40, 1002, 10.1029/2000RG000095, 2002.

Revel-Rolland M., De Deckker P., Delmonte, B., Hesse, P. P., Magee, J. W., Basile-Doelsch, I., Grousset, F., and Bosch, D.: Eastern Australia: A possible source of dust in East Antarctica interglacial ice, Earth Plant. Sc. Lett., 249, 1–13, 2006.

Roeckner, E., Brokopf, R., Esch, M., Giorgetta, M., Hagemann, S., and Kornblueh, L.: Sensitivity of simulated climate to horizontal and vertical resolution in the ECHAM5 atmosphere model, J. Climate, 19, 3771–3791, 2006.

Schüpbach, S., Federer, U., Kaufmann, P. R., Albani, S., Barbante, C., Stocker, T. F., and Fischer, H.: High-resolution mineral dust and sea ice proxy records from the Talos Dome ice core, Clim. Past, 9, 2789–2807, 10.5194/cp-9-2789-2013, 2013.

Smith, B., Prentice, I. C., and Sykes, M. T.: Representation of vegetation dynamics in the modelling of terrestrial ecosystems: comparing two contrasting approaches within European cli-

mate space, Global Ecol. Biogeogr., 10, 621–637, 10.1046/j.1466-822X.2001.t01-1-00256.x, 2001.

Sokolik, I. N., Winker, D. M., Bergametti, G., Gillette, D. A., Carmichael, G., Kaufman, Y. J., Gomes, L., Schuetz, L., and Penner, J. E.: Introduction to special section: outstanding problems in quantifying the radiative impacts of Triangle, J. Geophys. Res., 106, 18015–18027, 2001.

Stier, P., Feichter, J., Kinne, S., Kloster, S., Vignati, E., Wilson, J., Ganzeveld, L., Tegen, I., Werner, M., Balkanski, Y., Schulz, M., Boucher, O., Minikin, A., and Petzold, A.: The aerosol-climate model ECHAM5-HAM, Atmos. Chem. Phys., 5, 1125–1156, 10.5194/acp-5-1125-2005, 2005.

Tegen, I.: modelling the mineral dust aerosol cycle in the climate system, Quaternary Sci. Rev., 22, 1821–1834, 10.1016/S0277-3791(03)00163-X, 2003.

Tegen, I., Harrison, S. P., Kohfeld, K., Prentice, I. C., Coe, M., and Heimann, M.: Impact of vegetation and preferential source areas on global dust aerosol: Results from a model study, J. Geophys. Res., 107, 10.1029/2001JD000963, 2002.

Textor, C., Schulz, M., Guibert, S., Kinne, S., Balkanski, Y., Bauer, S., Berntsen, T., Berglen, T., Boucher, O., Chin, M., Dentener, F., Diehl, T., Easter, R., Feichter, H., Fillmore, D., Ghan, S., Ginoux, P., Gong, S., Grini, A., Hendricks, J., Horowitz, L., Huang, P., Isaksen, I., Iversen, I., Kloster, S., Koch, D., Kirkevåg, A., Kristjansson, J. E., Krol, M., Lauer, A., Lamarque, J. F., Liu, X., Montanaro, V., Myhre, G., Penner, J., Pitari, G., Reddy, S., Seland, Ø., Stier, P., Takemura, T., and Tie, X.: Analysis and quantification of the diversities of aerosol life cycles within AeroCom, Atmos. Chem. Phys., 6, 1777–1813, 10.5194/acp-6-1777-2006, 2006.

Twohy, C. H., Kreidenweis, S. M., Eidhammer, T., Browell, E. V., Heymsfield, A. J., Bansemer, A. R., Anderson, B. E., Chen, G., Ismail, S., DeMott, P. J., and Van Den Heever, S. C.: Saharan dust particles nucleate droplets in eastern Atlantic clouds, Geophys. Res. Lett., 36, L01807, 10.1029/2008GL035846, 2009.

Verheggen, B., Cozic, J., Weingartner, E., Bower, K., Mertes, S., Connolly, P., Gallagher, M., Flynn, M., Choularton, T., and Baltensperger, U.: Aerosol partitioning between the interstitial and the condensed phase in mixed-phase clouds, J. Geophys. Res., 112, D23202, 10.1029/2007JD008714, 2007.

Werner, M., Tegen, I., Harrison, S. P., Kohfeld, K. E., Prentice, I. C., Balkanski, Y., Rodhe, H., and Roelandt, C.: Seasonal and interannual variability of the mineral dust cycle under present and glacial climate conditions, J. Geophys. Res., 107, 4744,

10.1029/2002JD002365, 2002.

Wolff, E. W., Hall, J. S., Mulvaney, R., Pasteur, E. C., Wagenbach, D., and Legrand, M.: Relationship between chemistry of air, fresh snow and firn cores for aerosol species in coastal Antarctica, J. Geophys. Res., 103, 11057–11070, 10.1029/97JD02613, 1998.

Wolff, E. W., Fischer, H., Fundel, F., Ruth, U., Twarloh, B., Littot, G. C., Mulvaney, R., Röthlisberger, R., de Angelis, M., Boutron, C. F., Hansson, M., Jonsell, U., Hutterli, M. A., Lambert, F., Kaufmann, P., Stauffer, B., Stocker, T. F., Steffensen, J. P., Bigler, M., Siggaard-Andersen, M. L., Udisti, R., Becagli, S., Castellano, E., Severi, M., Wagenbach, D., Barbante, C., Gabrielli, P., and Gaspari, V.: Southern Ocean sea-ice extent, productivity and iron flux over the past eight glacial cycles, Nature, 440, 491–496, 10.1038/nature04614, 2006.

Zobler, L.: A world soil file for global climate modelling, Tech. Rep. NASA TM-87802, 1986.

26

Table 1. Orbital parameters and greenhouse gas concentrations for the CTRL, 6 kyr, 21 kyr, 115 kyr, 126 kyr simulations derived from the PMIP2 protocol.

	CTRL	6 kyr	21 kyr	115 kyr	126 kyr
eccentricity	0.016724	0.018682	0.018994	0.041421	0.03971
obliquity, [°]	23.446	24.105	22.949	22.404	23.928
day of perihelion	282.04	180.87	294.42	290.88	111.24
CO_2, [ppm]	280	280	185	280	280
CH_4, [ppm]	0.76	0.65	0.35	0.76	0.76
N_2O, [ppm]	0.27	0.27	0.20	0.27	0.27

Table 2. Global mass budget for different climate conditions.

	CTRL	6 kyr	115 kyr	126 kyr	LGM
Emissions, [Tg yr^{-1}]					
Total	1540	1961	1898	2385	3106
NH	1478	1845	1834	2273	946
SH	62	117	65	112	160
Australia	60	115	63	110	84
Southern America	1	1.1	1.2	1.2	75
Southern Africa	1.2	0.9	1.1	0.8	1.6
Deposition, [Tg yr^{-1}]					
Total dep.	1539	1959	1896	2376	3119
Wet dep.	643	828	790	1123	1293
Dry dep.	214	296	239	363	456
Sedimentation	682	835	867	890	1370
Deposition in Antarctica, [Tg yr^{-1}]					
Total dep.	0.053	0.150	0.061	0.141	0.540
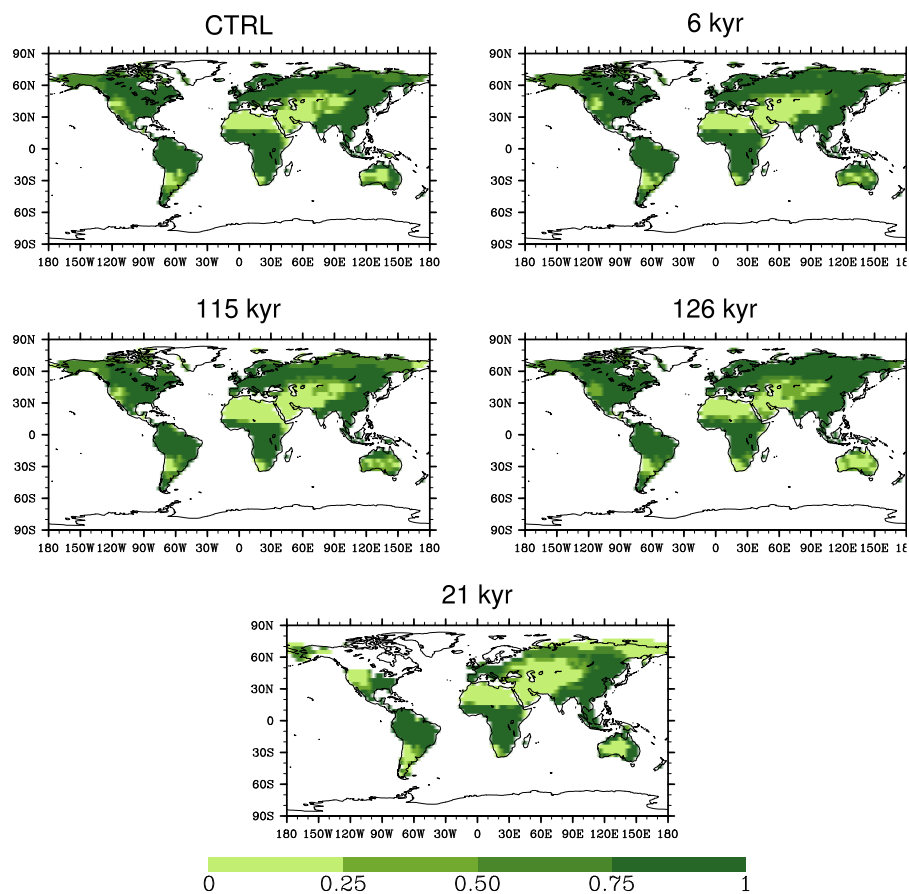
Fig. 1. Annual maximum vegetation cover fraction obtained from the LPJ-GUESS model for the CTRL, 6 kyr, 115 kyr, 126 kyr and LGM time periods. The regions with annual maximum vegetation cover less than or equal to 25 % (light green color) are defined as the potential dust source regions.
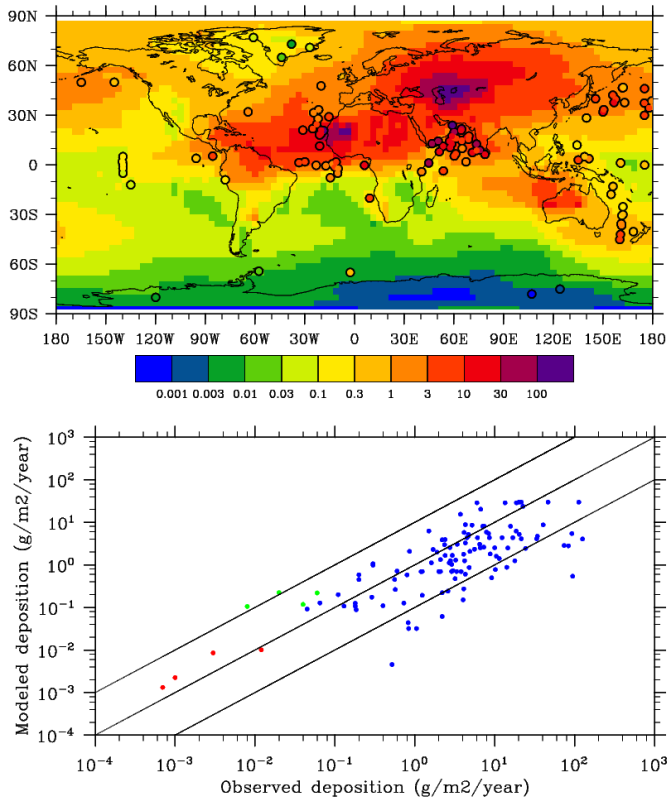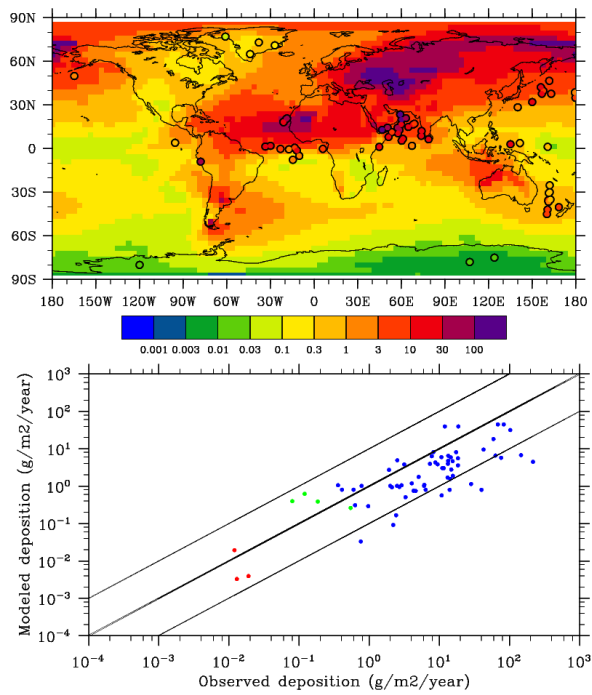
Fig. 2. Simulated dust deposition flux [$\mathrm{g\,m^{-2}\,yr^{-1}}$] for the pre-industrial time-slice compared with dust deposition data compiled from ice cores, marine sediment traps and marine sediment cores [$\mathrm{g\,m^{-2}\,yr^{-1}}$] (circles) and a scatter plot between the model and observations. The red color indicates Antarctica, green indicates Greenland and blue indicates other locations.
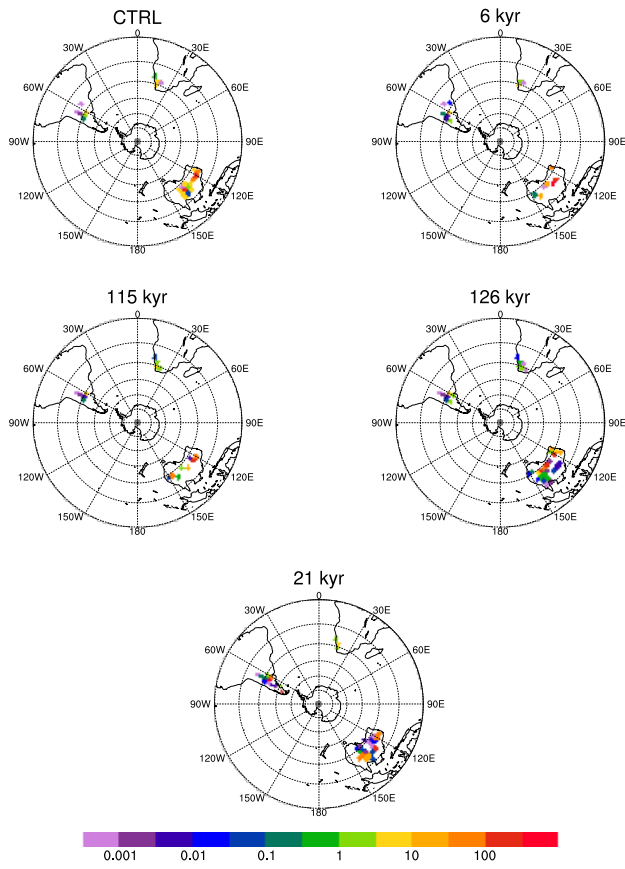
Fig. 3. Mean Southern Hemisphere dust emission flux for the CTRL, 6 kyr, 115 kyr, 126 kyr and LGM simulations, $[\mathrm{g\,m^{-2}\,yr^{-1}}]$.
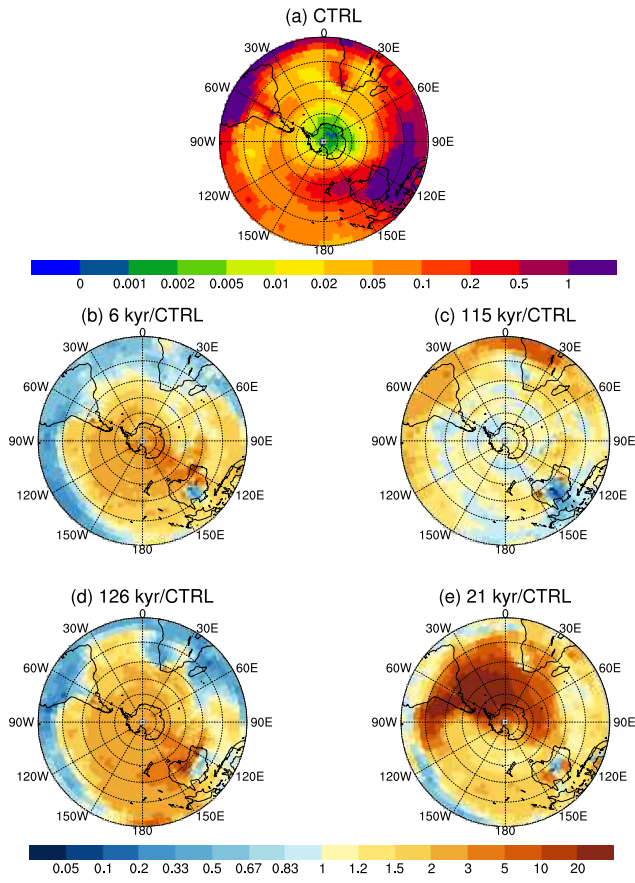
Fig. 4. Annual average dust deposition flux [$\mathrm{g\,m^{-2}\,yr^{-1}}$] for the Southern Hemisphere for the CTRL pre-industrial simulation **(a)**. Ratio of dust deposition flux for the interglacial and glacial time-slices with respect to the CTRL pre-industrial simulation **(b–e)**.

Fig. 5. Simulated dust deposition flux $[\mathrm{gm}^{-2}\mathrm{yr}^{-1}]$ for the LGM time-slice compared with dust deposition data compiled from ice cores, marine sediment traps and marine sediment cores $[\mathrm{gm}^{-2}\mathrm{yr}^{-1}]$ (circles) and a scatterplot between the model and observations. The red color indicates Antarctica, green indicates Greenland and blue indicates other locations.
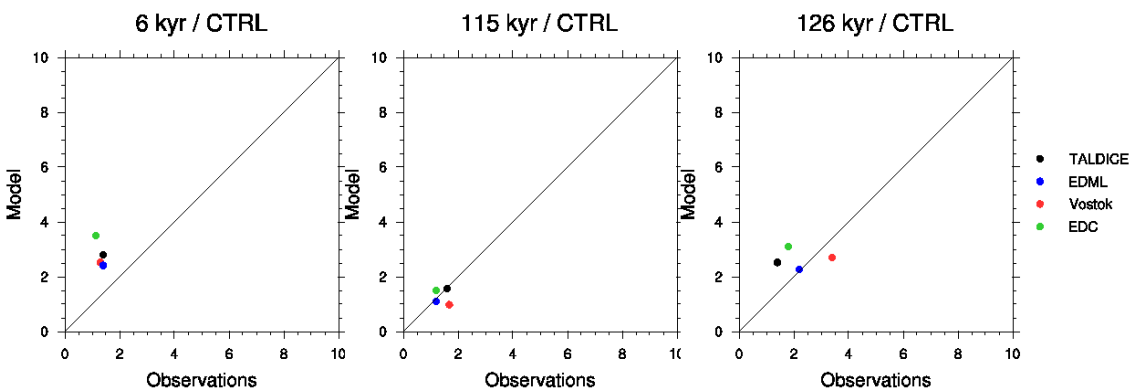
33
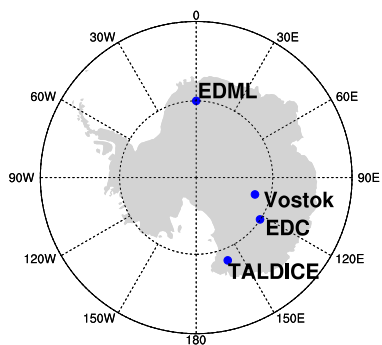
Fig. 6. Locations of the ice core sites in Antarctica.

Fig. 7. Dust deposition flux ratios of 6 kyr (left), 115 kyr (central) and 126 kyr (right) to pre-industrial period from observations and model simulations. Ratios are compared for four Antarctic cites, EDC (green), Vostok (red), EDML (blue) and TALDICE (black).
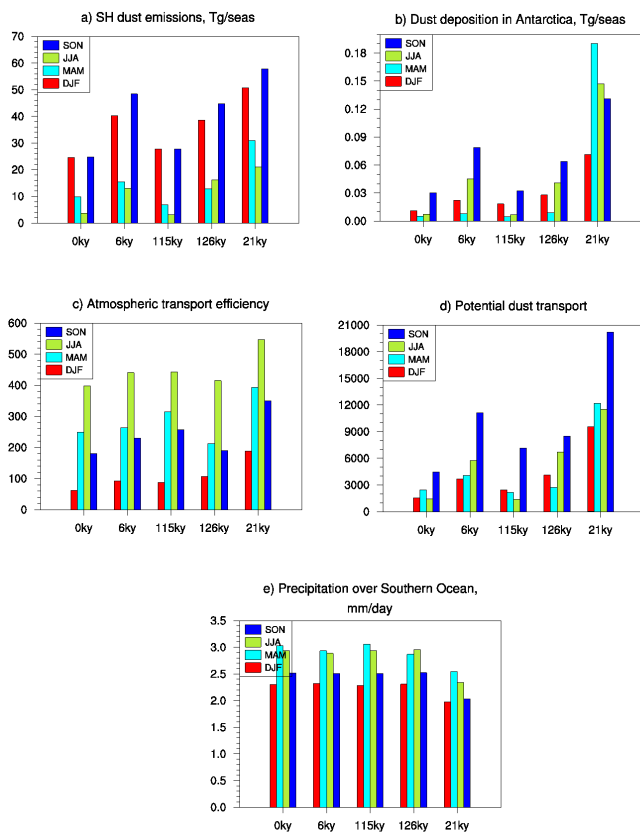
Fig. 8. **(a)** Southern Hemisphere dust emission [Tg season^{-1}], **(b)** dust deposition in Antarctica [Tg season^{-1}], **(c)** atmospheric transport efficiency [trajectories season^{-1}], **(d)** potential dust transport [arbitrary units], **(e)** precipitation over the ocean south of 40° S [mm day^{-1}] for the interglacial and glacial simulations. Atmospheric transport efficiency is the number of trajectories originated at 500 hPa and 800 hPa (combined) from a single dust source grid box per season and reached Antarctica within 10 days.
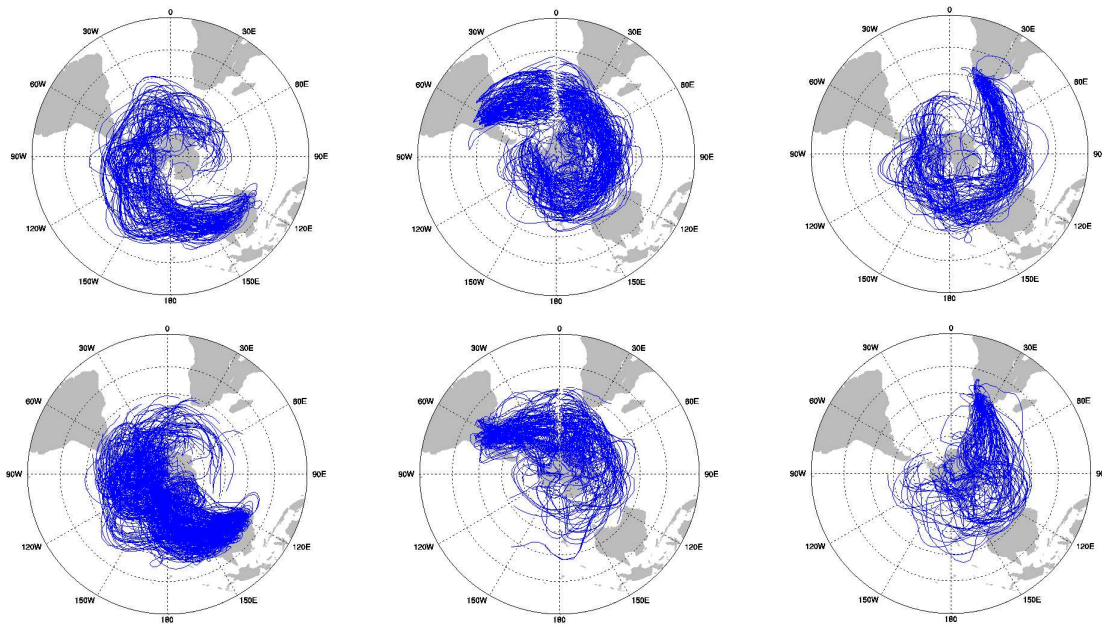
35

Fig. 9. Ten day forward trajectories of air masses originated at 500 hPa (top) and 800 hPa (bottom). Trajectories originated over the Australian (left), South American (central) and south African (right) dust sources and reached Antarctica withim 10 days. Trajectories are shown for the CTRL simulation, austral spring season (SON). Note that only every 2nd trajectory is plotted.
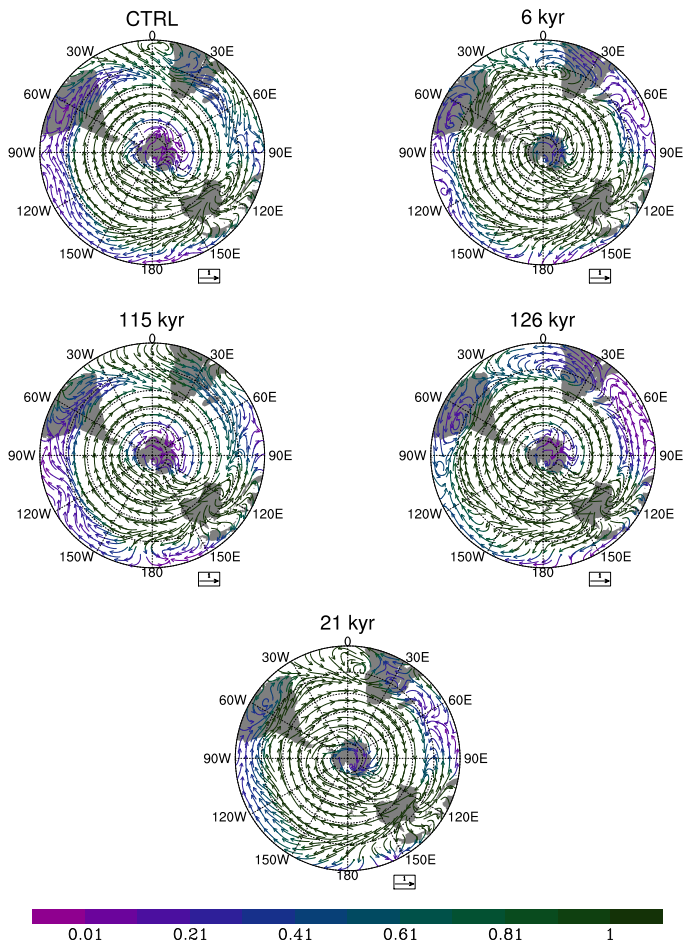
Fig. 10. Dust transport on 500 hPa calculated by using 6 hourly data, September, October, November (SON).
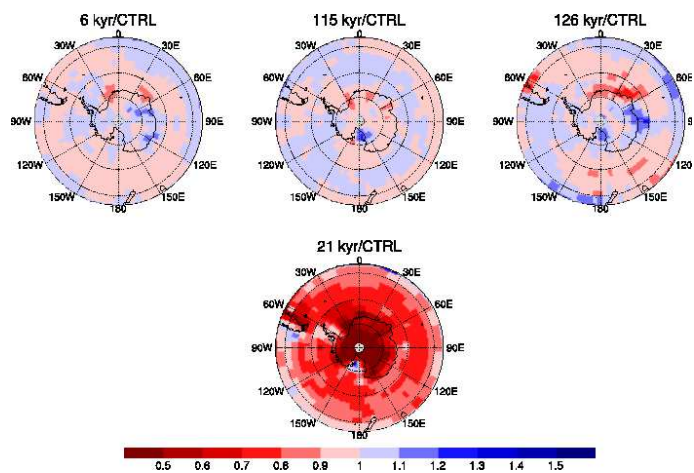
Fig. 11. Paleo to pre-industrial ratios of annual mean precipitation.